Nanoscale

Accepted Manuscript

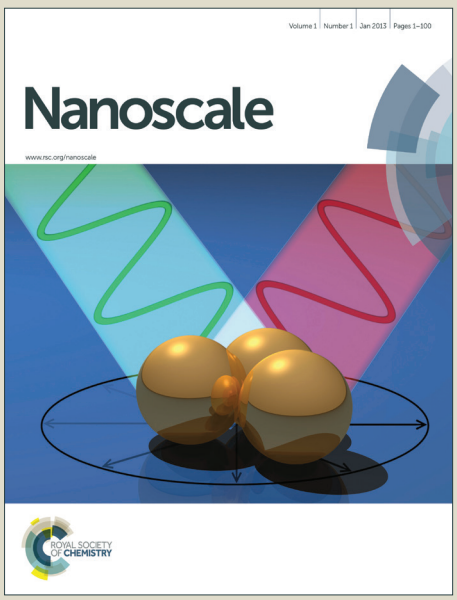

This is an *Accepted Manuscript*, which has been through the Royal Society of Chemistry peer review process and has been accepted for publication.

Accepted Manuscripts are published online shortly after acceptance, before technical editing, formatting and proof reading. Using this free service, authors can make their results available to the community, in citable form, before we publish the edited article. We will replace this *Accepted Manuscript* with the edited and formatted *Advance Article* as soon as it is available.

You can find more information about *Accepted Manuscripts* in the Information for Authors.

Please note that technical editing may introduce minor changes to the text and/or graphics, which may alter content. The journal's standard Terms & Conditions and the Ethical guidelines still apply. In no event shall the Royal Society of Chemistry be held responsible for any errors or omissions in this *Accepted Manuscript* or any consequences arising from the use of any information it contains.

ROYAL SOCIETY OF CHEMISTRY

www.rsc.org/nanoscale

Nanoscale

RSCPublishing

ARTICLE

Tuning Band Gaps of BN Nanosheets and Nanoribbons via Interfacial Dihalogen Bonding and External Electric Field

Cite this: DOI: 10.1039/xoxxoooooox

Qing Tang,[a,b] Jie Bao,[a] Yafei Li,[c] Zhen Zhou*[a] and Zhongfang Chen*[b]

Received ooth January 2012,
Accepted ooth January 2012

DOI: 10.1039/xoxxoooooox

www.rsc.org/

Density functional theory computations with dispersion corrections (DFT-D) were performed to investigate the dihalogen interactions and their effect on electronic band structures of halogenated (fluorinated and chlorinated) BN bilayers and aligned halogen-passivated zigzag BN nanoribbons (BNNRs). Our results reveal the presence of considerable homo-halogen (F···F and Cl···Cl) interactions in bilayer fluoro (chloro)-BN sheets and the aligned F (Cl)-ZBNNRs, as well as substantial hetero-halogen (F···Cl) interactions in hybrid fluoro-BN/chloro-BN bilayer and F-Cl-ZBNNRs. The existence of interfacial dihalogen interactions leads to significant band-gap modifications for the studied BN nanosystems. Compared with the individual fluoro (chloro)-BN monolayers or pristine BNNRs, the gap reduction in bilayer fluoro-BN (B-F···F-N array), hybrid fluoro-BN/chloro-BN bilayer (N-F···Cl-N array), aligned Cl-ZBNNRs (B-Cl···Cl-N alignment), and hybrid F-Cl-ZBNNRs (B-F···Cl-N alignment) is mainly due to interfacial polarizations, while the gap narrowing in bilayer chloro-BN (N-Cl···Cl-N array) is ascribed to the interfacial nearly-free-electron states. Moreover, the binding strengths and electronic properties of the interactive BN nanosheets and nanoribbons can be controlled by applying an external electric field, and an extensive modulation from large-gap to medium-gap semiconductors, or even metals can be realized by adjusting the direction and strength of the applied electric field. This interesting strategy for band gap control based on weak interactions offers unique opportunities for developing BN nanoscale electronic devices.

Introduction

Dihalogen bonding (halogen–halogen interaction) is a type of non-covalent interaction that occurs between two halogen atoms. The halogens X involved in dihalogen bonding typically include F, Cl, Br, and I, and the strength of X···X interaction increases with the general trend of F < Cl < Br < I. Dihalogen bonds occur due to the polarization of halogen atoms, and in a reasonable sense, F has a low polarizability so that the attractive F···F dispersion force should be rather weak as compared with heavier halogens (less electronegative and more polarizable). Actually, various intermolecular dihalogen bonds, such as homo-halogen (X···X, X = F,[1] Cl,[2] Br,[3] I) and hetero-halogen (F···X, X = Cl, Br, I)[4] interactions, do exist in molecular crystals with considerable stabilization energy, and these weak interactions have invoked extensive theoretical investigations.[5-9] Like other non-covalent interactions (such as hydrogen bonding, π-π stacking, and anion (cation)-π interaction), dihalogen bonding also plays a vital role in directing supramolecular packing for crystal engineering purposes.

Despite the growing interest in dihalogen bonding, much attention to this kind of non-covalent interaction has been paid to organic structures, and it is particularly desirable to extend this emerging subject into constructing functional nanostructures. Recently, layered hexagonal boron nitride (*h*-BN),[10,11] one isoelectronic and isostructural analogue of graphene, has attracted extensive studies in materials science, because of its novel properties (such as superb thermal stability and chemical inertness, extraordinary mechanical robustness, and electrically-insulating properties) and great potential for high-quality nanodevices (solid lubricant films in harsh conditions,[12] ultraviolet-light laser devices,[13] field emitters,[14] and insulating thermoconductive fillers[15]). Experimentally, two-dimensional (2D) mono- to few-layered BN nanosheets have been successfully produced via diverse bottom-up[16-18] and top-down[19-22] fabrication techniques. It is noteworthy that, in contrast to graphene sheet which is characterized as a zero-band-gap semimetal, BN sheets are typical wide-band-gap semiconductors (band gap: 5~6 eV) due to the strong ionicity of B-N bonds.[23] Moreover, enthused by the edge-driven fascinating properties of graphene nanoribbons, researchers have also devoted much interest to the derived one-dimensional (1D) BN nanoribbons (BNNRs), which can be experimentally synthesized by unzipping of BN nanotubes (the produced BNNRs mainly display zigzag-type edges).[24-26] However,

Nanoscale Accepted Manuscript

all types of BNNRs with edges passivated by hydrogen obtained experimentally still remain insulating.[27]

The large band gaps in BN-based materials constitute a major issue for their extensive applications, and it is highly desirable to control the band gaps of BN systems. So far, numerous methods have been developed to mediate the wide band gaps of BN nanosheets and BNNRs, such as doping,[28,29] defects,[30-32] applying electric field[27] and strain,[33] as well as chemical modifications.[34-38]

Beside the above mentioned approaches, weak interactions act as a new band modification tool. The most recent theoretical studies have revealed that, when two hydrogenated BN nanosheets or two hydrogen-passivated zigzag BNNRs are packed together, considerable interfacial B-H···H-N dihydrogen bonding would emerge.[39,40] Such weak interactions at the 2D or 1D interface can effectively modify the electronic structures of BN nanosystems, wherein the aligned BN nanosheets and polar zigzag BNNRs are sensitively tailored from insulators to narrow-band-gap semiconductors.[39,40] Motivated by the significant role of H···H interactions in tuning the band gaps of aligned BN nanostructures, it is then of great interest to investigate the effect of halogen-halogen interactions (dihalogen bonding) on the electronic structures of 2D BN sheets and 1D BNNRs. The idea of halogen-halogen interaction is somewhat similar to that of the hydrogen-hydrogen interaction, and both can be treated as the Lewis acid-base interaction; however, dihydrogen bondig and dihalogen bonding are different in nature. The dihydrogen bonding (described as A-H$^{\delta+}$···$^{\delta-}$H-B, where A is a strongly electronegative atom such as O or N, and B is a less electronegative element than H such as B, Al or Re), is a special kind of hydrogen bond, which is driven by the electrostatic attraction between two oppositely charged H atoms (the positively charged H acts as Lewis acid, while the negatively charged H acts as Lewis base). For dihalogen bonding (A-X···X-B, X usually designates a Cl, Br or I atom, and the two interactive X atoms can be neutral or charged), the X center can act as Lewis acid or as Lewis base owing to the anisotropy of the electron charge distribution of the halogen atom. Dihalogen interaction can be explained by the presence of a region of positive electrostatic potential (the so-called σ-hole) on the outermost surface of the halogen atom (σ-hole acts as Lewis acid, while another halogen atom acts as Lewis base). The σ-hole strength changes with the polarizability of the halogen atom, and hence the dihalogen bond strength can be tuned by changing the X centers.

In this work, we performed density functional theory (DFT) investigations on the halogenated (fluorinated and chlorinated) BN bilayers and halogen-passivated zigzag BNNRs (the zigzag edges are passivated by F or Cl). We paid close attention to the interfacial halogen-halogen interactions and the corresponding binding strengths between two interactive BN monolayers and the aligned zigzag BNNRs, and further studied the electronic structure changes that arise from the bilayer formation and ribbon alignment.

Computational method

Dispersion-corrected DFT (DFT-D) computations were performed using the DMol^3 code,[41,42] and the computations are based on the generalized gradient approximation (GGA)[43] treated by Perdew–Burke–Ernzerhof (PBE) exchange-correlation potential with long-range dispersion correction via Grimme's scheme.[44] Our benchmark computations of a bilayer BN sheet using this DFT-D method predict an interlayer distance of 3.36 Å, which is in good agreement with the experimental data (3.33-3.35 Å).[45,46] The double numerical plus polarization (DNP) basis set was employed. The real-space global cutoff radius was set to be 4.10 Å, and the self-consistent field (SCF) procedure was used with a convergence threshold of 10^{-6} au on the total energy. The nearest distance between the halogenated BN sheet (passivated BNNR) and its periodic images is greater than 16.0 Å. The Brillouin zones are sampled by 6 special k-points setting for geometry optimizations, and 24 special k-points are used for electronic structure computations. The k-point sampling was done by the Monkhorst-Pack scheme (Γ centred). In this work, the charge analysis is determined by using the Hirshfeld method[47] unless mentioned otherwise. Moreover, we also used the Heyd-Scuseria-Ernzerhof (HSE06)[48] screened exchange hybrid functional (implemented in Vienna *ab initio* simulation package (VASP)) to re-evaluate the band structure of hybrid fluoro-BN/chloro-BN bilayer. The reliability of this method has been tested in our previous work,[40] and the HSE computed band gap of single layer BN (benchmark computation) is 5.64 eV, in good agreement with the experimental value (5.97 eV).

Results and Discussion

Halogenated BN monolayers

Different from hydrogenated BN in which the boat- or stirrup-type structure is more favorable,[40] the fluorinated or chlorinated BN monolayer (denoted as fluoro-BN and chloro-BN) has a chair-type ground-state configuration (Fig. 1(a)). The fluorination or chlorination energy, defined as the energy difference between fluoro-BN or chloro-BN and the pristine BN and atomic F or Cl, is computed to be –2.64 eV/F atom and –0.19 eV/Cl atom, respectively. In comparison, the computed formation energies for F_2 and Cl_2 molecules are –2.51 and 2.77 eV, respectively. Thus, both atomic and molecular fluorination of BN are energetically exothermic; however, though atomic chlorination of BN is also exothermic, molecular chlorination is endothermic. Thus, for the fully chlorinated BN sheets, the attached Cl might desorb and form molecules, and in reality, partial chlorination should be favored. Note that full functionalization with perfectly and periodically attached functional groups is an ideal process in theory, partial functionalization with randomly distributed groups might be more likely in practical chemical processes. In this work, the focus is the F···F and Cl···Cl interactions and their impacts on the band gap tuning of BN systems, accordingly we first concentrated on the fully functionalized structures, then studied the partially functionalized BN monolayer and bilayer sheets to show that the trend for fully functionalized systems also holds true in partially functionalized systems.

To confirm the thermodynamic stability of fluoro- and chloro-BN, we computed their phonon vibration frequencies, and in the phonon dispersion curve (Fig. S1, Electronic Supplementary Information (ESI)), all branches of phonon spectrum are positive and no

Nanoscale Accepted Manuscript

imaginary phonon mode exists, implying that both fluoro-BN and chloro-BN are true local minima.

Moreover, the resulting fluoro-BN and chloro-BN monolayers are direct-band-gap semiconductors, with reduced band gaps (3.56 eV for fluoro-BN and 1.09 eV for chloro-BN) as compared with the pristine BN monolayer (4.79 eV at the same computational level).

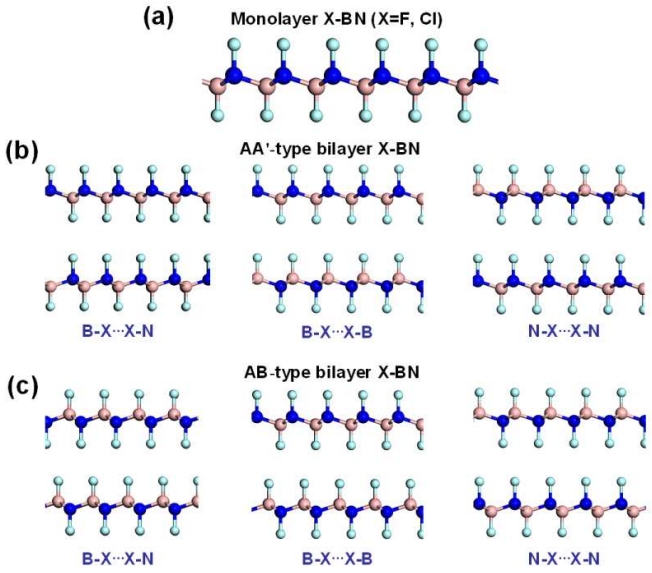

Fig. 1 Structure of (a) monolayer fluoro-BN or chloro-BN, and (b,c) high-symmetry fluoro- or chloro-BN bilayer configurations with interlayer B-X···X-N, B-X···X-B, and N-X···X-N (X= F, Cl) arrangements, respectively. The orange, blue, and light blue balls represent B, N and X atoms, respectively.

Homo dihalogen bonding between halogenated BN layers

When the layer-by-layer stacking is considered for halogenated BN bilayers, the halogen atoms spanning along the 2D interface can form X···X dihalogen bonding in or between two BN layers. We examined six high-symmetry arrangements of bilayer fluoro-BN and chloro-BN with AA'- or AB-type arrayed B-X···X-N, B-X···X-B, and N-X···X-N (X= F, Cl) overlapping modes (Fig. 1b and 1c). Note that for AA'-type stacking of *h*-BN, the B (N) atoms of one layer sit directly above or below the N (B) atoms of the other layer, while in the case of AB-type stacking, the B (N) atoms in one layer are located above or below the center of a hexagon.

Total energy computations showed that the energy difference between the most stable stacking configuration and the least stable one is 16.3 meV per unit cell for fluoro-BN bilayer and 57.2 meV per unit cell for chloro-BN bilayer (Table 1), respectively. Moreover, fluoro-BN bilayer prefers the AB-type B-F···F-N interlayer connection, whereas chloro-BN bilayer favors the AB-type N-Cl···Cl-N interactions. In the most favorable stacking patterns, our computations predict an interlayer separation (distance between two interactive X planes) of 2.49 Å and a layer binding energy of 78.9 meV per unit cell for fluoro-BN bilayer, and an interlayer separation of 2.98 Å and a layer-binding energy of 149.7 meV per unit cell for chloro-BN bilayer. The two interactive F layers or Cl layers are both found to carry uniform negative charge, and the interlayer F···F or Cl···Cl attraction should be contributed by the polarization-induced van der Waals (vdW) forces. In particular, the Cl···Cl interaction in chloro-BN bilayer (binding energy of 92.5 to 149.7 meV per unit cell) is much stronger than the F···F interaction in fluoro-BN bilayer (binding energy of 62.6 to 78.9 meV per unit cell), which is possibly due to the larger polarization of Cl atoms. Note that different systems prefer different stacking orders. The favorable B-F···F-N binding (staggered AB stacking) for fluoro-BN bilayer should be mainly ascribed to strong interfacial polarization (the interactive B-F and N-F bonds possess different polarities, and the polarization of the B-F···F-N interface is even stronger than that of the B-Cl···Cl-N interface, see the discussion below), which leads to larger polarized interactions between the heterogeneous B-F and F-N bonds than those between the homogeneous B-F and F-B or N-F and F-N bonds. While for chloro-BN bilayer, the interfacial N-Cl···Cl-N binding becomes the most favorable, which indicates that charge repulsion plays a more significant role than the interface polarization. Our charge analysis shows that the Cl atoms bonded to B and N atoms carry negative charge of about 0.06 and 0.01 |e|, respectively, thus, the N-$Cl^{\sigma-\cdots\sigma-}$Cl-N interaction should be favored due to larger repulsive interactions at B-$Cl^{\sigma-\cdots\sigma-}$Cl-N and B-$Cl^{\sigma-\cdots\sigma-}$Cl-B interfaces. Moreover, the binding energy of fluoro-BN and chloro-BN bilayers in their unit cells (corresponding to a single F···F or Cl···Cl bond) is much larger than room-temperature thermal perturbation energy (25 meV). With increasing structural sizes or areas, more interactive F···F or Cl···Cl bonds would be involved, and the binding energy would become even larger. Thus, these stacked bilayer structures, once formed, would be stable against thermal perturbation.

Table 1 Interlayer separations d_{sep} [Å] (the c-lattice parameter), binding energies E_{bind} [meV per unit cell], and band gaps E_{gap} [eV] of bilayer fluoro-BN and bilayer chloro-BN with different stacking patterns. The results corresponding to the energetically most favorable configuration are marked in bold.

		AA'(AB)-type bilayer		
		B-X···X-N	B-X···X-B	N-X···X-N
fluoro-BN	d_{sep}	2.76 (**2.49**)	2.51 (2.52)	2.50 (2.50)
	E_{bind}	62.6 (**78.9**)	73.5 (73.5)	70.7 (70.7)
	E_{gap}	2.67 (**2.64**)	3.51 (3.51)	3.29 (3.29)
chloro-BN	d_{sep}	3.43 (3.10)	3.25 (3.19)	2.99 (**2.98**)
	E_{bind}	92.5 (127.9)	106 (106)	146.9 (**149.7**)
	E_{gap}	0.54 (0.54)	0.98 (1.01)	0.57 (**0.60**)

The electronic structure computations revealed that the presence of interlayer weak interactions in bilayer counterparts induces band-gap modifications (Table 1), which is strongly dependent on the

Nanoscale Accepted Manuscript

interacting modes. As a general trend, the band gaps of bilayer structures are smaller than those of the monolayer ones, and the band-gap reduction follows the order as: B-X···X-N > N-X···X-N > B-X···X-B (X=F, Cl), regardless of the AA'- or AB-stacked pattern. Specifically, the band gaps of bilayer fluoro-BN with AA'- (AB-) type interlayer B-F···F-N, N-F···F-N, and B-F···F-B geometries are 2.67 (2.64) eV, 3.29 (3.29) eV, and 3.51 (3.51) eV, respectively, which correspond to the gap reduction of 0.89 (0.92) eV, 0.27 (0.27) eV, and 0.05 (0.05) eV as compared with the monolayer fluoro-BN (E_g: 3.56 eV). Similarly, the band gaps of bilayer chloro-BN with AA'- (AB-) type interlayer B-Cl···Cl-N, N-Cl···Cl-N, and B-Cl···Cl-B geometries are 0.54 (0.54) eV, 0.57 (0.60) eV, and 0.98 (1.01) eV, respectively, which correspond to the gap reduction of 0.55 (0.55) eV, 0.52 (0.49) eV, and 0.11 (0.08) eV as compared with the monolayer chloro-BN (E_g: 1.09 eV).

Particularly, the band gaps of fluoro-BN bilayers with interactive B-F···F-N configurations (AA' or AB) are significantly reduced compared with their B-F···F-B or N-F···F-N counterparts. The difference in their electronic structures might be attributed to the different interfacial polarization: significant polarization occurs in the asymmetric B-F···F-N interactions, almost negligible polarization exist in the symmetric B-F···F-B or N-F···F-N interactions. Note that the interfacial polarization is induced by the interlayer B-F···F-N interactions, with the F atoms bonded to B-layer and N-layer carrying unequivalent negative charge [~0.11 |e| for F(B) and ~0.05 |e| for F(N)]. In a reasonable sense, the more negative F(B) atoms would donate some electrons to the less negative F(N) atoms to compensate the interfacial polarization. Actually, atomic charge analysis reveals that there is an interlayer charge transfer of about 0.002|e| per difluorine bond from F(B) to F(N) in B-F···F-N-arrayed bilayer fluoro-BN, while no charge transfer is observed between the two BN layers in their B-F···F-B or N-F···F-N counterparts. Similarly, there is also an interlayer charge transfer (about 0.001 |e| per unit cell) in bilayer chloro-BN with B-Cl···Cl-N patterns, and no charge transfer occurs in the B-Cl···Cl-B or N-Cl···Cl-N arrayed conformers. Moreover, we also used Bader charge analysis to check the B-F···F-N and B-Cl···Cl-N arrayed structures, and the computed interface charge transfer is 0.003|e| and 0.001|e| per unit cell, respectively, nearly consistent with the results of Hirshfeld charge analysis. Note that the induced interface charge transfer is extremely small and negligible, and is beyond the accuracy of charge population calculations. However, the qualitative conclusion derived from charge analysis is expected to be reliable: the charge transfer at the B-F···F-N interface is slightly larger than that at the B-Cl···Cl-N interface. The larger charge transfer is accompanied by a larger band gap reduction (the reduced band gap is 0.92 eV for fluoro-BN and 0.55 eV for chloro-BN after forming AB stacked bilayers), which indicates a stronger interfacial polarization for fluoro-BN bilayer.

To better understand the effect of interfacial polarization to the band gap reduction, we plotted the profile of plane-averaged electrostatic potential along the normal direction of B-F(Cl)···F(Cl)-N arrayed fluoro-BN and chloro-BN bilayer (Fig. 2). A considerable potential difference can be observed around the 2D interface, which is up to 0.93 eV (fluoro-BN bilayer) and 0.57 eV (chloro-BN bilayer) in the profiles, comparable to the decreased band gap of fluoro-BN and chloro-BN after forming bilayers. For both fluoro-BN and chloro-BN bilayers, the electrostatic potential of the upper fluoro-BN or chloro-BN layer (the inverted left layer in Fig. 2) is lifted relative to that of the bottom layer (the inverted right layer in Fig. 2). As a result, the energy level of the upper layer is shifted upward as compared to that of the bottom layer, giving rise to a staggered band lineup and thus a reduced band gap (as illustrated in the inset of Fig. 2(a)). In this case, the band gap is formed by the highest occupied state (HO state) of the upper layer and the lowest unoccupied state (LU state) of the bottom layer, consistent with the charge density analysis in Fig. 3b and f. Thus the presence of interfacial polarization should play a dominant role in reducing the band gaps of B-X···X-N-arrayed BN nanosheets. In particular, note that bilayer chloro-BN with N-Cl···Cl-N arrangement (without interlayer charge transfer) exhibits nearly comparable band gap to its B-Cl···Cl-N conformer, and the remarkable gap reduction in N-Cl···Cl-N pattern might be due to interlayer nearly free electron (NFE) states (Fig. 3h), which will be discussed later.

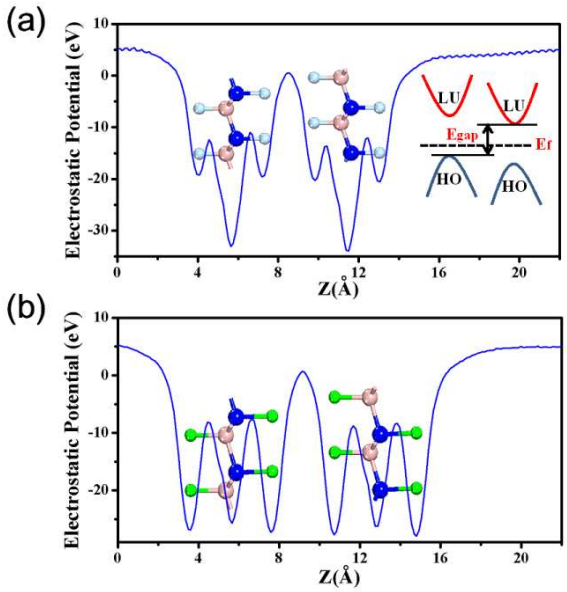

Fig.2 Plane-averaged electrostatic potential along the normal direction of AB stacked fluoro-BN bilayer (a) and chloro-BN bilayer (b) with interface B-X···X-N configurations. The inset in (a) is a schematic illustration of a staggered band lineup between two BN bilayers induced by interface polarization. The light blue and green balls represent F and Cl atoms, respectively.

To further understand the geometry-dependent electronic properties, we present the band structures of monolayer and AB-typed bilayer fluoro-BN and chloro-BN (the AA'-typed structures demonstrate similar results to the AB-typed ones), respectively, together with their partial charge densities corresponding to the HO state and the LU state at the Γ point (Fig. 3). Note that all the considered monolayer and bilayer fluoro(chloro)-BN systems are direct-band-gap semiconductors, and both the valence band maximum (VBM) and conduction band minimum (CBM) are located at the Γ point.

In monolayer fluoro-BN, the HO state is from the sp^3-bonded B-N, B-F, and N-F bonding states, and the LU state is mainly from the

Nanoscale Accepted Manuscript

N-F anti-bonding states (with a little contribution from the B-F anti-bonding states). In this case, the LU state mainly distributes out of the BN sheet and has a feature resembling the surface NFE state that has been known in layered systems and in fluorinated graphene.[49]

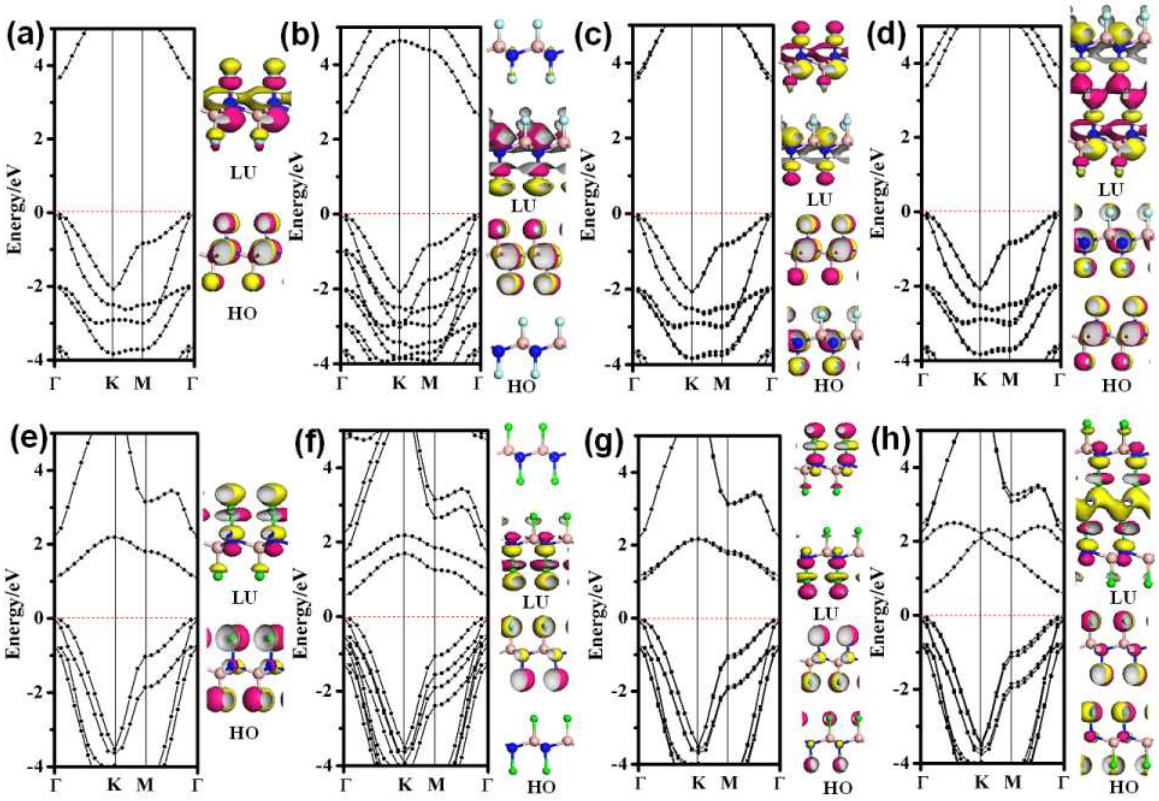

Fig. 3 Band structures and partial charge densities of HO and LU states at the Γ point for monolayer fluoro-BN (a), AB-stacked bilayer fluoro-BN with interlayer B-F···F-N (b), B-F···F-B (c), and N-F···F-N (d) connections. (e)-(h) correspond to the results for monolayer chloro-BN, AB-stacked bilayer chloro-BN with interlayer B-Cl···Cl-N, B-Cl···Cl-B, and N-Cl···Cl-N connections, respectively.

Upon the formation of fluoro-BN bilayer, the wave functions of HO and LU states become strongly geometry-dependent. Specifically, because of interfacial polarization, the HO and LU states of B-F···F-N-arrayed fluoro-BN show asymmetric distribution and are differently separated onto one of the BN planes. By contrast, the HO and LU states of B-F···F-B- and N-F···F-N-arrayed fluoro-BN are symmetrically distributed over the two separated BN layers. Note that the HO state of B-F···F-B-arrayed fluoro-BN has similar bonding character to the N-F···F-N-arrayed conformer, yet their LU states are notably different, wherein a strongly delocalized NFE-like state exists in or between the N-F···F-N interlayer. The NFE state is located at the conduction band edge, which shifts the level of CBM downward and decreases the band gap, and this explains the smaller band gap of N-F···F-N-arrayed bilayer fluoro-BN than its B-F···F-B counterpart.

The charge density distributions of monolayer and bilayer chloro-BN are very similar to the fluoro-BN counterparts. Particularly, because of the larger polarization of Cl atoms, the surface NFE-like character of the LU state (from the N-Cl anti-bonding states) of chloro-BN becomes more labile, which leads to the stronger downshift of CBM state and thus rapidly reduces the band gap of N-Cl···Cl-N-arrayed bilayer chloro-BN. In addition, we also checked the NFE state computed through plane-wave basis set (VASP code). Fig. S2 presents the VBM and CBM distributions at the Γ point for monolayer and bilayer fluoro-BN or chloro-BN with different stacking configurations. Similar to the results of atomic basis set, the interface NFE state is only in the CBM of N-X···X-N-arrayed structures, and the N-Cl···Cl-N-arrayed structure exhibits a much stronger interface NFE sate than the N-F···F-N-arrayed one.

Therefore, the interfacial polarization dominates the gap reduction of B-X···X-N-arrayed BN nanosheets, while the NFE state at the conduction band edge contributes to the gap reduction of N-X···X-N-arrayed ones. The B-X···X-B-arrayed structures, however, remain almost unaffected as compared with their monolayer counterparts.

Moreover, we also studied the partially functionalized BN monolayer and bilayer sheets (see Fig. S3) to check if the obtained trend of band gap reduction based on fully functionalized BN systems also hold true for partially functionalized BN monolayer and bilayer sheets. Our results show that the band gaps of partially fluorinated BN monolayers are smaller than the fully fluorinated BN,

Nanoscale Accepted Manuscript

and the band gaps are inclined to increase with the increasing fluorination ratio. Unlike the case of partial fluorination, the band gaps of partially chlorinated BN monolayers become larger than the fully chlorinated one, and the band gaps tend to decrease with the increasing chlorination ratio. In both cases, the band gaps of partially fluorinated or chlorinated BN bilayers (with arrayed B-F···F-N and N-Cl···Cl-N interfaces, respectively) are smaller than the partially functionalized BN monolayers. Therefore, the presence of interlayer F···F and Cl···Cl interactions also results in the band gap reduction of partially functionalized BN sheets, and the electronic structures of BN sheets can be tuned in a wide scope by changing the fluorination or chlorination ratios.

Hetero dihalogen bonding between halogenated BN layers

Our above discussion only focused on the homo-halogen (F···F and Cl···Cl) interactions. Herein, we additionally studied the hetero-halogen (F···Cl) interactions between fluoro-BN and chloro-BN. The hybrid fluoro-BN/chloro-BN bilayer energetically prefers the AB stacked N-F···Cl-N arrangement (Fig. 4(a)), and the consequential layer binding of 383.7 meV (per unit cell) is drastically stronger than those homogeneous F···F and Cl···Cl bindings. Such a strong N-F···Cl-N binding should be contributed by both the vdW interaction and the Coulomb attraction, wherein the interface F(N) and Cl(N) atoms are found to carry negative charge of 0.089 |e| and positive charge of 0.021 |e|, respectively, leading to considerable electrostatic attraction between the two oppositely charged planes.

Moreover, the computed band structures indicated that the arrayed fluoro-BN/chloro-BN bilayer becomes metallic, with the conduction band edge (near the Γ point) slightly crossing the Fermi level (Fig. 4(b)). Considering the band gap underestimation of GGA-PBE functional, we used the HSE06 to examine the above mentioned system. The HSE06 computations predicted a small band gap of 0.03 eV for the hybrid fluoro-BN/chloro-BN bilayer (Fig. 4(c)), which is amazingly smaller than the band gap of the pristine fluoro-BN or chloro-BN monolayer. Note that the standard HSE06 with a mixing parameter of 0.25 has shown good results for most systems. Herein we also checked the HSE06 computations with a different mixing parameter. When a lower mixing parameter (0.2 and 0.15) is used, the fluoro-BN/chloro-BN bilayer still remains semiconducting with a similar band gap of 0.03 eV (Fig. S4), which confirms the narrow-band-gap semiconducting character of the hybrid fluoro-BN/chloro-BN bilayer. According to the charge density analysis (Fig. 4(d)), the HO state of the hybrid system mainly derives from the chloro-BN layer, while the LU state is distributed uniformly onto the fluoro-BN/chloro-BN bilayer. Compared with the B-F···F-N- and B-Cl···Cl-N-arrayed BN bilayers, the dramatically lower band gap of the N-F···Cl-N-arrayed hybrid fluoro-BN/chloro-BN should be ascribed to its stronger interfacial polarization, which is accompanied by a large interlayer charge transfer (about 0.03 e per unit cell) from chloro-BN to fluoro-BN (Fig. 4(a)).

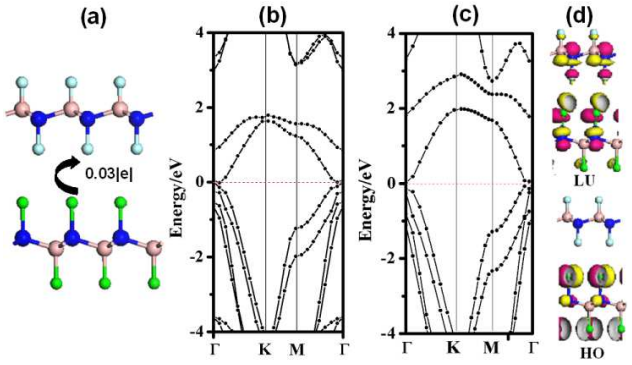

Fig. 4 Geometry structure (a), band structure (b at the GGA level, c at the HSE06 level), as well as the HO and LU states (d) of the N-F···Cl-N-arrayed fluoro-BN/chloro-BN bilayer.

Dihalogen bonding between halogen-passivated BN nanoribbons

Following the investigation on halogenated BN nanosheets, we then diverted our attention to the halogen-passivated zigzag BN nanoribbons. Herein, we use the notation of n-X-ZBNNR to specify a zigzag BNNR with n parallel zigzag chains along the ribbon width, wherein both the B and N edges are saturated by X atoms (X=F, Cl). When two X-ZBNNRs are aligned side by side, six interface connections (parallel-aligned and mis-aligned or staggered B-X···X-N, B-X···X-B, N-X···X-N structures) might exist (Fig. 5).

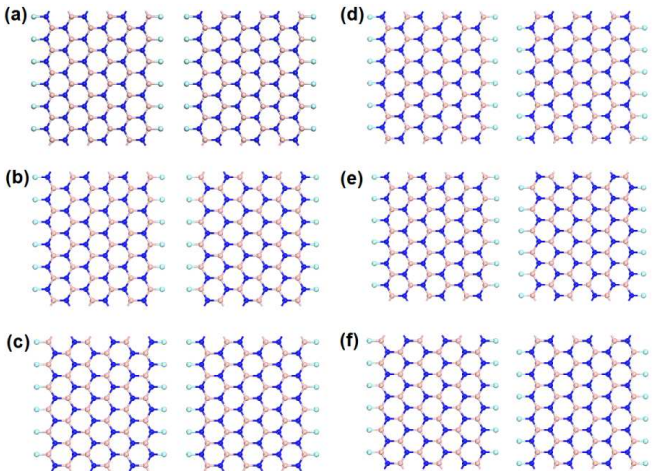

Fig. 5 Aligned 6-X-ZBNNRs with different interfacial structures: (a)-(c) correspond to the parallel-aligned B-X···X-N, B-X···X-B, and N-X···X-N geometries, while (d)-(f) correspond to the mis-aligned or staggered B-X···X-N, B-X···X-B, and N-X···X-N geometries, respectively.

Total energy computations indicate that the two units of F-passivated ZBNNRs prefer the staggered N-F···F-N interface alignment; in stark contrast, the Cl-passivated ZBNNRs energetically favor the staggered B-Cl···Cl-N configuration. Their difference in interfacial alignment can be understood by analysing the atomic charge. For F-ZBNNRs, the F atoms bonded to edge N and B atoms carry negative charge of about 0.06 |e| and 0.12 |e|, respectively, and thus N-F···F-N interaction is more favorable than B-F···F-B or B-F···F-N interaction due to larger interface repulsion of

Nanoscale Accepted Manuscript

the latter. Differently, for Cl-ZBNNRs, the Cl atoms bonded to edge N and B atoms are found to charge oppositely, which carry positive charge of 0.02 |e| and negative charge of 0.06 |e|, respectively. As a result, the attractive B-Cl$^{\delta-\cdots\delta+}$Cl-N interaction is energetically more preferable than the repulsive B-Cl$^{\delta-\cdots\delta-}$Cl-B or N-Cl$^{\delta+\cdots\delta+}$Cl-N interaction.

The interfacial binding energy of the two interactive X-ZBNNRs, denoted as n-X-ZBNNR-2, exhibits strong width dependence, which decreases with increasing the ribbon width (Fig. 6(a)). As a trend, the interfacial Cl···Cl interactions (60.9 to 15.1 meV per unit cell as width n increases from 3 to 14, the red line in Fig. 6(a)) are much stronger than the interfacial F···F interactions (28.6 to 6.08 meV per unit cell as width n increases from 3 to 14, the black line in Fig. 6(a)) for the aligned n-X-ZBNNRs-2. Note that these aligned X···X interactions occur at the 1D interfaces of BN nanoribbons are much weaker than those occurred at the 2D interfaces of stacked BN nanosheets.

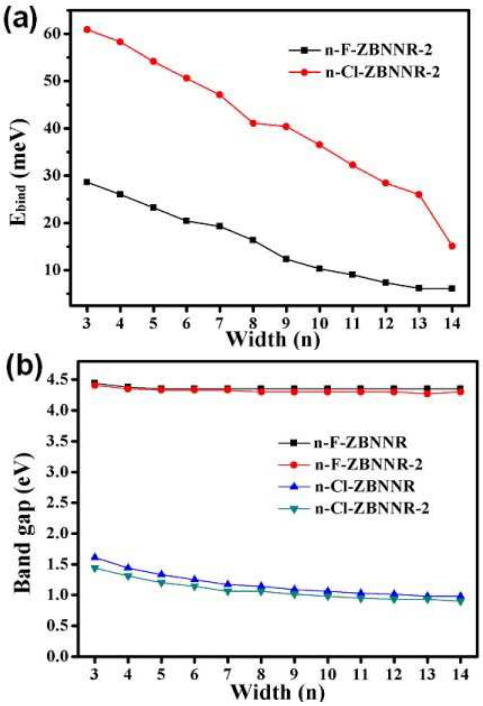

Fig. 6 (a) The interface binding energy (E_{bind}, per unit cell) of two interactive X-ZBNNRs (n-X-ZBNNR-2) as a function of the width parameter n. The black square corresponds to n-F-ZBNNR-2 with staggered N-F···F-N interface, while the red circle corresponds to n-Cl-ZBNNR-2 with staggered B-Cl···Cl-N interface. (b) Band gaps of n-X-ZBNNR (black square for n-F-ZBNNR and blue triangle for n-Cl-ZBNNR) and n-X-ZBNNR-2 (red circle for n-F-ZBNNR-2 with staggered N-F···F-N interface, while the dark cyan triangle for n-Cl-ZBNNR-2 with staggered B-Cl···Cl-N interface) as functions of n.

To examine whether the presence of interfacial X···X interactions might impact on the electronic properties of BN nanoribbons, in Fig. 6b we present the computed band gaps of a single n-X-ZBNNR and two aligned n-X-ZBNNRs as functions of the width parameter n. The single and aligned n-F-ZBNNRs are all wide-band-gap semiconductors, and they have very close band gaps that finally converge to be about 4.35 eV (for n-F-ZBNNR, the black line in Fig. 6(b)) and 4.30 eV (for n-F-ZBNNR-2, the red line in Fig. 6(b)) as width increases. This observation indicates that the aligned F-ZBNNRs exhibit similar electronic structures to the individual F-ZBNNRs. Interestingly, different from the case of F-ZBNNRs, the aligned Cl-ZBNNRs all have slightly reduced band gaps as compared with their single Cl-ZBNNRs. Specifically, the band gap of the single Cl-ZBNNRs is 1.61 eV for 3-Cl-ZBNNR and 0.98 eV for 14-Cl-ZBNNR (the blue line in Fig. 6(b)), respectively, which is then reduced to 1.44 eV for 3-Cl-ZBNNR-2 and 0.90 eV for 14-Cl-ZBNNR-2 (the dark cyan line in Fig. 6(b)) when the interface is composed of B-Cl···Cl-N alignments. The larger band gaps for the narrower ribbons should be an indication of quantum confinement effect.

In order to understand their difference in electronic properties, we plotted the band structures and charge density distributions corresponding to 7-F-ZBNNR, 7-F-ZBNNR-2 (N-F···F-N alignment), and 7-Cl-ZBNNR, 7-Cl-ZBNNR-2 (B-Cl···Cl-N alignment). As shown in Fig. 7, the single 7-F-ZBNNR (Fig. 7(a)) has a large indirect band gap of 4.35 eV, the VBM state is at the Y point and the CBM state is along the Γ→Y point; in comparison, the single 7-Cl-ZBNNR (Fig. 7(c)) has a moderate direct band gap of 1.17 eV, both the VBM and CBM states are located at the Γ point. After forming the side-by-side alignments, the resulting 7-F-ZBNNR-2 (Fig. 7(b)) and 7-Cl-ZBNNR-2 (Fig. 7(d)) have band gaps of 4.33 eV and 1.06 eV, respectively.

In the 7-F-ZBNNR, the HO state is mainly contributed by the π state of edge N-F bonds, while the LU state is mainly from the π* state of edge B-F bonds. In the N-F···F-N-aligned 7-F-ZBNNR-2, the locations of the HO and LU states remain almost unchanged, and both are symmetrically distributed onto the two aligned 7-F-ZBNNRs. This may explain the similarity in electronic structures between 7-F-ZBNNR and 7-F-ZBNNR-2. In the case of 7-Cl-ZBNNR, the HO state is highly located at the σ orbital of N-Cl edges, while the LU state is located at the π* orbital of B-Cl edges. In the B-Cl···Cl-N-aligned 7-Cl-ZBNNR-2, the HO state is located at the interfacial N-Cl edges, while the LU state is located at the non-interface B-Cl edges, and they are both exclusively distributed onto one of the interactive ribbons. The asymmetrical HO and LU distributions lead to disruption of the energy-level degeneracy (each energy level is split into two-fold levels), which shifts the VBM (CBM) upward (downward) and slightly decreases the band gap.

Nanoscale Accepted Manuscript

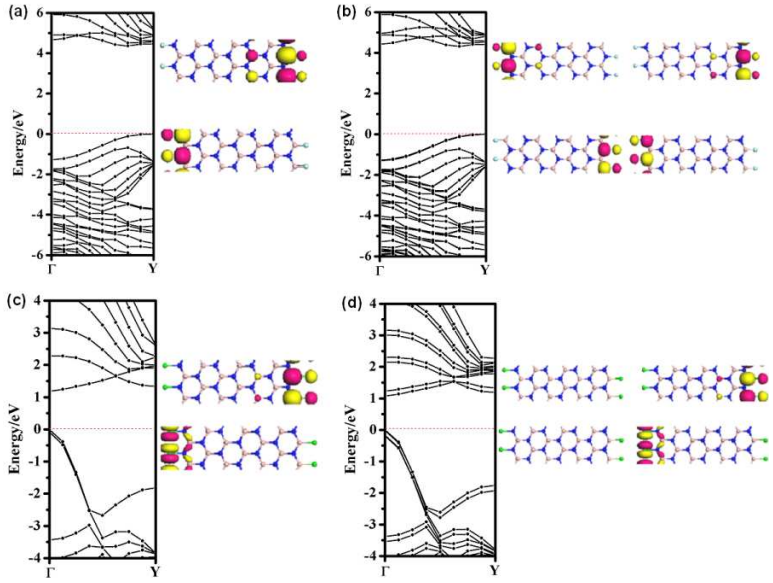

Fig. 7 Band structures (left) and electronic profile of the HO state (right lower) and the LU state (right upper) for 7-F-ZBNNR (a), 7-F-ZBNNR-2 (N-F···F-N alignment) (b), 7-Cl-ZBNNR (c), and 7-Cl-ZBNNR-2 (B-Cl···Cl-N alignment) (d), respectively.

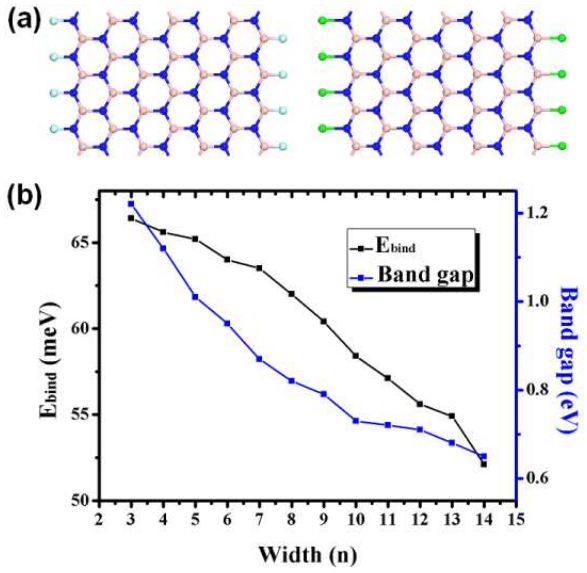

Fig. 8 (a) Aligned 7-F-Cl-ZBNNR with B-F···Cl-N interface geometry. (b) The interfacial binding energy (black square) and band gap (blue square) of hybrid n-F-Cl-ZBNNR as a function of n.

In addition, similar to the investigation of hybrid fluoro-BN/chloro-BN nanosheets, we further studied hybrid BN nanoribbons composed of aligned n-F-ZBNNR and n-Cl-ZBNNR (denoted as n-F-Cl-ZBNNR). In light of the structural stability, the hybrid F-Cl-ZBNNRs favor the staggered B-F···Cl-N interface alignments (Fig. 8(a)). The favorable B-F···Cl-N alignment mainly derives from B-$F^{\delta-\cdots\delta+}$Cl-N electrostatic attraction, which is stronger than the N-$F^{\delta-\cdots\delta+}$Cl-N alignment since the F atoms bonded to B carry more negative charge, thus inducing stronger F···Cl attraction. The optimal interfacial binding energy of F-Cl-ZBNNRs decreases as the ribbon parameter n increases (from 66.4 meV per unit cell for 3-F-Cl-ZBNNR to 52.1 meV per unit cell for 14-F-Cl-ZBNNR, as indicated by the black line in Fig. 8(b)), and the E_{bind} is much stronger than that in N-F···F-N- or B-Cl···Cl-N-aligned ZBNNRs. This demonstrates the sufficiently high binding stability between F-ZBNNRs and Cl-ZBNNRs. Moreover, the band gap of hybrid n-F-Cl-ZBNNR decreases as n increases (from 1.22 eV for 3-F-Cl-ZBNNR to 0.65 eV for 14-F-Cl-ZBNNR, as indicated by the blue line in Fig. 8(b)). Note that the band gaps of hybrid F-Cl-ZBNNRs are smaller than those of the N-F···F-N aligned F-ZBNNRs or B-Cl···Cl-N aligned Cl-ZBNNRs. These hybrid F-Cl-ZBNNRs are indirect-band-gap semiconductors (taking 7-F-Cl-ZBNNR as an example, which has an indirect-band-gap of 0.87 eV, Fig. 9(a)), and the HO and LU states are exclusively contributed by the interface N-Cl edge of Cl-ZBNNR unit and the interface B-F edge of F-ZBNNR unit, respectively (Fig. 9(b)). Similar to B-Cl···Cl-N aligned ZBNNRs, the asymmetric HO and LU distributions for B-F···Cl-N aligned F-Cl-ZBNNRs result from interface polarization.

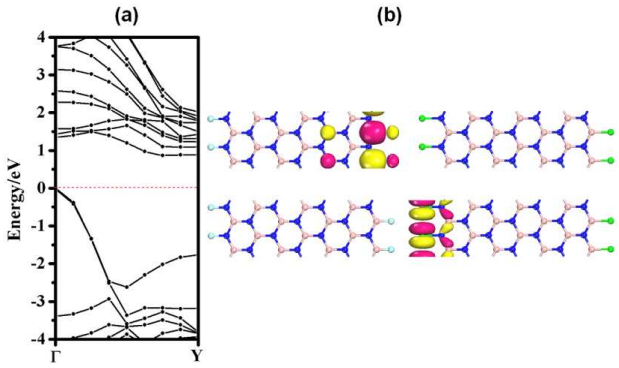

Fig. 9 (a) Band structure and (b) electronic profile (HO and LU states) of the hybrid 7-F-Cl-ZBNNR.

Nanoscale Accepted Manuscript

Tuning the band gap by applying external electric field

Applying external electric field (E_{ext}) has proven a useful tool for achieving tunable electronic behaviors in low-dimensional nanostructures. Recently, the external electric field has also been used to enhance the interfacial binding in hydrogen-functionalized BN bilayers and nanoribbons,[39,40] as well as the binding between graphane and fluorographene bilayer.[50] Motivated by these studies, we further examined the electric field effect (the positive electric field is defined as the arrow direction in Fig. 10) on the binding strengths and electronic properties of aligned BN nanosheets (B-F···F-N- and N-Cl···Cl-N-arrayed BN bilayers, as well as the N-F···Cl-N-arrayed fluoro-BN/chloro-BN bilayer) and ZBNNRs (7-F-ZBNNR-2, 7-Cl-ZBNNR-2, and hybrid 7-F-Cl-ZBNNR).

As shown in Fig. 10a, with an applied negative electric field, the E_{bind} of bilayer fluoro-BN (the black line in Fig. 10(a)) increases significantly within the calculated range of electric fields and reaches up to 88.6 meV at E_{ext} of -0.25 V/Å; in contrast, with an applied positive electric field, the E_{bind} firstly increases to 82.7 meV at a field strength of 0.05 V/Å, and then decreases gradually with the increase of E_{ext} (71.2 meV at E_{ext} of 0.3 V/Å). Similar to bilayer fluoro-BN, the E_{bind} of bilayer chloro-BN (the red line in Fig. 10(a)) is weakened by imposing a positive field but becomes greatly enhanced by the negative field (up to 164.2 meV at a field around –0.3 V/Å). For the hybrid fluoro-BN/chloro-BN bilayer, the E_{bind} (the blue line in Fig. 10(a)) decreases with the applied positive field (78.5 meV at E_{ext} of 0.3 V/Å), while the E_{bind} first decreases and then increases rapidly with the applied negative field (624 meV at E_{ext} of -0.3 V/Å).

The situation for the aligned ZBNNRs (Fig. 10b) becomes more complicated. Regardless of the applied field direction, the E_{bind} of 7-F-ZBNNR-2 (the black line in Fig. 10(b)) and 7-Cl-ZBNNR-2 (the red line in Fig. 10(b)) first increases at a small field, then decreases to a minimum, and later increases with the rising positive or negative field. Under an appropriate electric field, the E_{bind} of ZBNNRs can be increased to 29.8 meV (7-F-ZBNNR-2 at E_{ext} of 0.05 V/Å) and 58.9 meV (7-Cl-ZBNNR-2 at E_{ext} of 0.05 V/Å). As for the hybrid 7-F-Cl-ZBNNR, the binding strength (the blue line in Fig. 10(b)) firstly decreases to 59.6 meV at E_{ext} of 0.1 V/Å and then increases with the increasing positive field (up to 103.7 meV at E_{ext} of 0.3 V/Å); while under a negative field, the E_{bind} firstly increases to 64.4 meV at E_{ext} of 0.05 V/Å and then becomes weakened with the increasing negative field.

Besides the adjustable binding energies, the applied electric field also provides an effective band gap engineering scheme for the arrayed BN bilayers and ZBNNRs (Fig. 11).

Clearly, the band gap of bilayer fluoro-BN (the black line in Fig. 11) decreases continuously with increasing positive electric field, which effectively reduces its large gap from 2.64 eV to 1.44 eV (E_{ext} = 0.3 V/Å). On the contrary, with an increasing negative electric field, the band gap of bilayer fluoro-BN initially increases and then turns to decrease when the E_{ext} exceeds a critical value (from 3.32 eV at E_{ext} = –0.2 V/Å to 3.1 eV at E_{ext} = –0.3 V/Å). For bilayer chloro-BN (the red line in Fig. 11), its band gap is slightly increased from 0.6 eV to 0.65 eV (–0.15 V/Å ≤ E_{ext} ≤ 0.3 V/Å) at a positive electric field, while the band gap becomes monotonically reduced under a negative electric field (0.16 eV at E_{ext} = –0.3 V/Å). Interestingly, the hybrid fluoro-BN/chloro-BN bilayer (the blue line in Fig. 11) becomes metallic within the applied negative field and the small positive field (0 V/Å ≤ E_{ext} ≤ 0.05 V/Å), and becomes semiconducting with a larger positive field (0.05 V/Å ≤ E_{ext} ≤ 0.3 V/Å), wherein the band gap increases with the positive electric field (up to 0.33eV at E_{ext} of 0.3 V/Å).

Moreover, regardless of the electric field direction, the band gaps of aligned ZBNNRs show a decreased tendency with the field strength, and their intrinsic gaps can be well tuned from 4.33 eV to 0.3 eV (E_{ext} = 0.3 V/Å) or 1.28 eV (E_{ext} = –0.3V/Å) for 7-F-ZBNNR-2 (the dark cyan line in Fig. 11), from 1.06 eV to metal (E_{ext} ≥ 0.2 V/Å) or to 0.11 eV (E_{ext} = –0.3 V/Å) for 7-Cl-ZBNNR-2 (the magenta line in Fig. 11), and from 0.87 eV to metal (E_{ext} ≥ 0.1 V/Å or -0.3 V/Å ≤ E_{ext} ≤ -0.15 V/Å) for the hybrid 7-F-Cl-ZBNNR (the dark yellow line in Fig. 11), respectively.

Nanoscale Accepted Manuscript

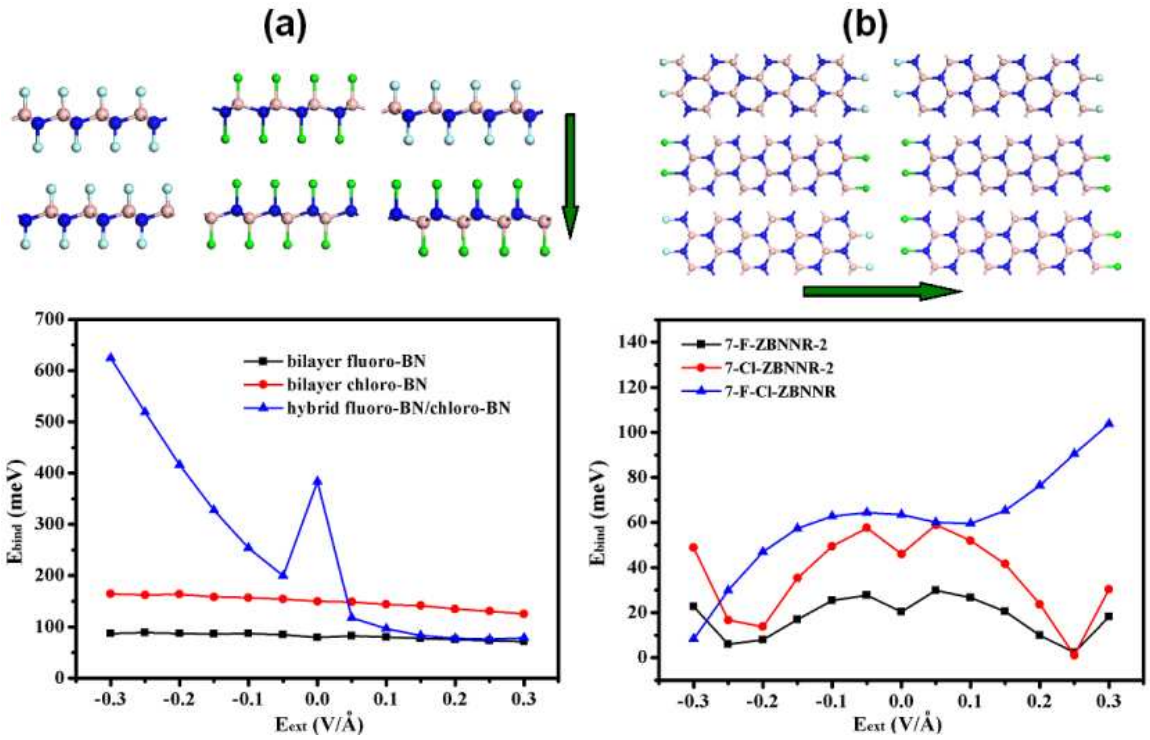

Fig. 10 Variation of the binding energy (E_{bind}, per unit cell) for the arrayed BN nanosheets [a, AB stacked bilayer fluoro-BN (black square) and chloro-BN (red circle), and the hybrid fluoro-BN/chloro-BN (blue triangle)] and aligned ZBNNRs [b, staggered 7-F-ZBNNR-2 (black square), 7-Cl-ZBNNR-2 (red circle), and the hybrid 7-F-Cl-ZBNNR (blue triangle)] as a function of the applied electric field strength. The positive direction of the applied electric field is denoted by the arrows.

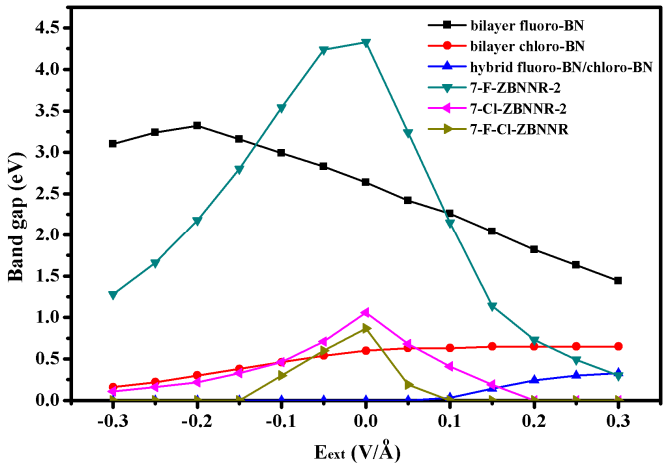

Fig. 11 Variation of the band gaps of bilayer fluoro-BN (black square), bilayer chloro-BN (red circle), hybrid fluoro-BN/chloro-BN (blue triangle), 7-F-ZBNNR-2 (dark cyan triangle), 7-Cl-ZBNNR-2 (magenta triangle) and hybrid 7-F-Cl-ZBNNR (dark yellow triangle) as a function of the external electric field strength.

Therefore, the electronic properties of the arrayed BN sheets or ribbons can be effectively controlled from large-gap to medium-gap semiconductors, or even converted to be metals by adjusting the direction and strength of the applied electric field. Such a wide-ranging gap modulation for the arrayed BN nanosystems opens a huge space for developing their functional applications in nanoelectronics.

Conclusion

In summary, our DFT-D computations demonstrate the existence of considerable halogen-halogen (F···F, Cl···Cl, and F···Cl) interactions between the halogenated BN bilayer sheets. Because of the larger polarization of Cl atoms, the interlayer Cl···Cl interactions are much stronger than the F···F counterparts. The presence of these dihalogen interactions induces substantial alterations on the electronic structures of wide-band-gap BN sheets. Compared with the individual fluoro-BN and chloro-BN monolayers (both having a large band gap), the fluoro-BN bilayer, which prefers the AB stacked B-F···F-N array, has a reduced band gap due to strong interfacial polarization, while the chloro-BN bilayer, which favors the AB stacked N-Cl···Cl-N array, exhibits a significantly reduced band gap due to the strongly delocalized interfacial NFE state. Moreover, the hybrid fluoro-BN/chloro-BN bilayer with interlayer N-F···Cl-N array possesses even much lower band gap because of its stronger interface polarization.

Besides the 2D BN sheets, dihalogen interactions also occur at the 1D interface of halogen-passivated zigzag BNNRs. However, the F···F, Cl···Cl, and F···Cl interactions arise between the two aligned ZBNNRs are significantly weaker than those between the stacked BN bilayers. Note that the band gaps of the aligned F-ZBNNRs (with preferable N-F···F-N interface alignment) remain nearly

Nanoscale Accepted Manuscript

unchanged as compared with the single F-ZBNNRs. By contrast, the aligned Cl-ZBNNRs with B-Cl···Cl-N interface geometries have lower band gaps than the single Cl-ZBNNRs, and the gap narrowing mainly arises from the interface polarization. Because of the interfacial polarizations, the hybrid F-Cl-ZBNNRs with B-F···Cl-N interface alignment also exhibit semiconducting band gaps smaller than the aligned F-ZBNNRs or aligned Cl-ZBNNRs.

Applying external electric field effectively modulates the binding strengths and electronic properties of the interactive BN nanosheets and nanoribbons, and an extensive modulation from large-band-gap to medium-band-gap semiconductor, or even metals can be realized by adjusting the direction and strength of the applied electric field. It is highly expected that the results of this theoretical study would shed some light on the possible ways to tune the band gaps of BN nanosystems and other wide-gap nanomaterials, and facilitate the design and fabrication of dihalogen-bonding-driven nanomaterials with promising applications.

Acknowledgements

Support in China by NSFC (21273118), 111 Project (B12015) and MOE Innovation Team (IRT13022), and in USA by Department of Defense (Grant W911NF-12-1-0083) is gratefully acknowledged.

Notes and references

[a] *Tianjin Key Laboratory of Metal and Molecule Based Material Chemistry, Key Laboratory of Advanced Energy Materials Chemistry (Ministry of Education), Computational Centre for Molecular Science, Institute of New Energy Material Chemistry, Collaborative Innovation Center of Chemical Science and Engineering (Tianjin), Nankai University, Tianjin 300071, P. R. China. Email: zhouzhen@nankai.edu.cn*

[b] *Department of Chemistry, Institute for Functional Nanomaterials, University of Puerto Rico, Rio Piedras Campus, San Juan, PR 00931. Email: zhongfangchen@gmail.com*

[c] *Nanjing Normal University, Department of Chemistry, Nanjing 210042, China*

Electronic Supplementary Information (ESI) available: [Phonon dispersion structures, partial charge densities, HSE06 band structures of various halogenated BN nanostructures.]. See DOI: 10.1039/b000000x/

1 R. Bayon, S. Coco and P. Espinet, *Chem. Eur. J.*, 2005, **11**, 1079-1085.
2 A. Matsumoto, T. Tanaka, T. Tsubouchi, K. Tashiro, S. Saragai and S. Nakamoto, *J. Am. Chem. Soc.*, 2002, **124**, 8891-8902.
3 R. Gutzler, C. Fu, A. Dadvand, Y. Hua, J. M. MacLeod, F. Rosei and D. F. Perepichka, *Nanoscale*, 2012, **4**, 5965-5971.
4 S. K. Nayak, M. K. Reddy, T. N. Guru Row and D. Chopra, *Cryst. Growth Des.*, 2011, **11**, 1578-1596.
5 R. B. K. Siram, D. P. Karothu, T. N. Guru Row and S. Patil, *Cryst. Growth Des.*, 2013, **13**, 1045-1049.
6 K. E. Riley, J. Rezac and P. Hobza, *J. Mol. Mod.*, 2013, **19**, 2879-2883.
7 J. Trnka, R. Sedlak, M. Kolar and P. Hobza, *J. Phys. Chem. A*, 2013, **117**, 4331-4337.
8 F. F. Awwadi, R. D. Willett, K. A. Peterson and B. Twamley, *Chem. Eur. J.*, 2006, **12**, 8952-8960.
9 R. J. Baker, P. E. Colavita, D. M. Murphy, J. A. Platts and J. D. Wallis, *J. Phys. Chem. A*, 2012, **116**, 1435-1444.
10 Y. Lin and J. W. Connell, *Nanoscale*, 2012, **4**, 6908-6939.
11 Q. Tang and Z. Zhou, *Prog. Mater. Sci.*, 2013, **58**, 1244-1315.
12 C. Lee, Q. Li, W. Kalb, X. Z. Liu, H. Berger, R. W. Carpick and J. Hone, *Science*, 2010, **328**, 76-80.
13 R. Gao, L. Yin, C. Wang, Y. Qi, N. Lun, L. Zhang, Y. Liu, L. Kang and X. Wang, *J. Phys. Chem. C*, 2009, **113**, 15160-15165.
14 Y. Zhu, Y. Bando, L. Yin and D. Golberg, *Nano Lett.*, 2006, **6**, 2982-2986.
15 C. Zhi, Y. Bando, C. Tang, H. Kuwahara and D. Golberg, *Adv. Mater.*, 2009, **21**, 2889-2893.
16 L. Song, L. Ci, H. Lu, P. B. Sorokin, C. Jin, J. Ni, A. G. Kvashnin, D. G. Kvashnin, J. Lou, B. I. Yakobson and P. M. Ajayan, *Nano Lett.*, 2010, **10**, 3209-3215.
17 A. Nag, K. Raidongia, K. P. S. S. Hembram, R. Datta, U. V. Waghmare and C. N. R. Rao, *ACS Nano*, 2010, **4**, 1539-1544.
18 X. Wang, C. Zhi, L. Li, H. Zeng, C. Li, M. Mitome, D. Golberg and Y. Bando, *Adv. Mater.*, 2011, **23**, 4072-4076.
19 D. Pacilé, J. C. Meyer, C. O. Girit and A. Zettl, *Appl. Phys. Lett.*, 2008, **92**, 133107.
20 Y. Lin, T. V. Williams and J. W. Connell, *J. Phys. Chem. Lett.*, 2010, **1**, 277-283.
21 J. N. Coleman, M. Lotya, A. O'Neill, S. D. Bergin, P. J. King, U. Khan, K. Young, A. Gaucher, S. De, R. J. Smith, I. V. Shvets, S. K. Arora, G. Stanton, H. Y. Kim, K. Lee, G. T. Kim, G. S. Duesberg, T. Hallam, J. J. Boland, J. J. Wang, J. F. Donegan, J. C. Grunlan, G. Moriarty, A. Shmeliov, R. J. Nicholls, J. M. Perkins, E. M. Grieveson, K. Theuwissen, D. W. McComb, P. D. Nellist and V. Nicolosi, *Science*, 2011, **331**, 568-571.
22 X. Li, X. Hao, M. Zhao, Y. Wu, J. Yang, Y. Tian and G. Qian, *Adv. Mater.*, 2013, **25**, 2200-2204.
23 K. Watanabe, T. Taniguchi and H. Kanda, *Nat. Mater.*, 2004, **3**, 404-409.
24 H. Zeng, C. Zhi, Z. Zhang, X. Wei, X. Wang, W. Guo, Y. Bando and D. Golberg, *Nano Lett.*, 2010, **10**, 5049-5055.
25 K. J. Erickson, A. L. Gibb, A. Sinitskii, M. Rousseas, N. Alem, J. M. Tour and A. K. Zettl, *Nano Lett.*, 2011, **11**, 3221-3226.
26 L. Li, L. H. Li, Y. Chen, X. J. Dai, P. R. Lamb, B. M. Cheng, M. Y. Lin and X. Liu, *Angew. Chem. Int. Ed.*, 2013, **52**, 4212-4216.
27 C. H. Park and S. G. Louie, *Nano Lett.*, 2008, **8**, 2200-2203.
28 X. Wei, M. S. Wang, Y. Bando and D. Golberg, *ACS Nano*, 2011, **5**, 2916-2922.
29 Q. Tang, Z. Zhou and Z. Chen, *J. Phys. Chem. C*, 2011, **115**, 18531-18537.
30 W. Chen, Y. Li, G. Yu, Z. Zhou and Z. Chen, *J. Chem. Theory. Comput.*, 2009, **5**, 3088-3095.
31 A. Du, Y. Chen, Z. Zhu, R. Amal, G. Q. Lu and S. C. Smith, *J. Am. Chem. Soc.*, 2009, **131**, 17354-17359.

Nanoscale Accepted Manuscript

32 X. Li, X. Wu, X. C. Zeng and J. Yang, *ACS Nano*, 2012, **6**, 4104-4112.
33 J. Qi, X. Qian, L. Qi, J. Feng, D. Shi and J. Li, *Nano Lett.*, 2012, **12**, 1224-1228.
34 W. Chen, Y. Li, G. Yu, C. Li, S. B. Zhang, Z. Zhou and Z. Chen, *J. Am. Chem. Soc.*, 2010, **132**, 1699-1705.
35 H. X. Zhang and P. X. Feng, *ACS Appl. Mater. Interfaces*, 2012, **4**, 30-33.
36 J. Zhou, Q. Wang, Q. Sun, P. Jena, *Phys. Rev. B*, 2010, **81**, 085442.
37 X. Wu, M. Wu, X. C. Zeng, *Front. Phys. China*, 2009, **4**, 367-372.
38 A. Lopez-Bezanilla, J. Huang, H. Terrones and B. G. Sumpter, *Nano Lett.*, 2011, **11**, 3267-3273.
39 Z. Zhang, W. Guo and B. I. Yakobson, *Nanoscale*, 2013, **5**, 6381-6387.
40 Q. Tang, Z. Zhou, P. Shen and Z. Chen, *ChemPhysChem*, 2013, **14**, 1787-1792.
41 B. Delley, *J. Chem. Phys.*, 1990, **92**, 508.
42 B. Delley, *J. Chem. Phys.*, 2000, **113**, 7756.
43 J. P. Perdew, K. Burke and M. Ernzerhof, *Phys. Rev. Lett.*, 1996, **77**, 3865-3868.
44 S. Grimme, *J. Comput. Chem.*, 2006, **27**, 1787-1799.
45 R. Pease, *Acta Crystallogr.*, 1952, **5**, 356-361.
46 Y. Shi, C. Hamsen, X. Jia, K. K. Kim, A. Reina, M. Hofmann, A. L. Hsu, K. Zhang, H. Li, Z. Y. Juang, M. S. Dresselhaus, L. J. Li and J. Kong, *Nano Lett.*, 2010, **10**, 4134-4139.
47 F. L. Hirshfeld, *Theor. Chim. Acta*, 1977, **44**, 129-138.
48 (a) J. Heyd, G. E. Scuseria and M. Ernzerhof, *J. Chem. Phys.*, 2003, **118**, 8207-8215. (b) J. Heyd and G. E. Scuseria, *J. Chem. Phys.*, 2004, **121**, 1187-1192.
49 N. Lu, Z. Li and J. Yang, *J. Phys. Chem. C*, 2009, **113**, 16741-16746.
50 Y. Li, F. Li and Z. Chen, *J. Am. Chem. Soc.*, 2012, **134**, 11269-11275.

Nanoscale Accepted Manuscript

Graphical Abstract

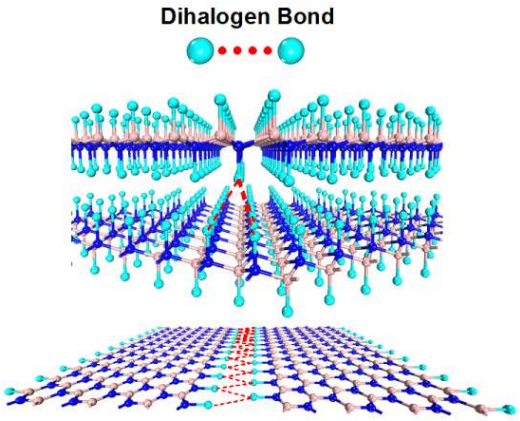

Nanoscale Accepted Manuscript